

# Carrier diffusion in GaN—a cathodoluminescence study. I: Temperature-dependent generation volume

Uwe Jahn,<sup>1</sup> Vladimir M. Kaganer,<sup>1</sup> Karl K. Sabelfeld,<sup>2</sup> Anastasya E. Kireeva,<sup>2</sup> Jonas Lähnemann,<sup>1</sup> Carsten Pfüller,<sup>1</sup> Caroline Chèze,<sup>1</sup> Klaus Biermann,<sup>1</sup> Raffaella Calarco,<sup>1,\*</sup> and Oliver Brandt<sup>1,†</sup>

<sup>1</sup>*Paul-Drude-Institut für Festkörperelektronik, Leibniz-Institut im  
Forschungsverbund Berlin e.V., Hausvogteiplatz 5–7, 10117 Berlin, Germany*

<sup>2</sup>*Institute of Computational Mathematics and Mathematical Geophysics,  
Russian Academy of Sciences, Lavrentiev Prosp. 6, 630090 Novosibirsk, Russia*

The determination of the carrier diffusion length of semiconductors such as GaN and GaAs by cathodoluminescence imaging requires accurate knowledge about the spatial distribution of generated carriers. To obtain the lateral distribution of generated carriers for sample temperatures between 10 and 300 K, we utilize cathodoluminescence intensity profiles measured across single quantum wells embedded in thick GaN and GaAs layers. Thin (Al,Ga)N and (Al,Ga)As barriers, respectively, prevent carriers diffusing in the GaN and GaAs layers to reach the well, which would broaden the profiles. The experimental CL profiles are found to be systematically wider than the energy loss distributions calculated by means of the Monte Carlo program CASINO, with the width monotonically increasing with decreasing temperature. This effect is observed for both GaN and GaAs and becomes more pronounced for higher acceleration voltages. We discuss this phenomenon in terms of the electron-phonon interaction controlling the energy relaxation of hot carriers, and of the non-equilibrium phonon population created by this relaxation process. Finally, we present a phenomenological approach to simulate the carrier generation volume that can be used for the investigation of the temperature dependence of carrier diffusion.

## I. INTRODUCTION

Scanning electron microscopy (SEM) enables a number of imaging, analytical and lithographical techniques with potentially high spatial resolution, as the electron beam can be focused down to 1 nm in modern field-emission microscopes [1, 2]. SEM is thus well suited and often the method of choice for the fabrication and investigation of nanostructures [3]. For a comprehensive physical and chemical characterization of these structures, various analytical techniques can be combined in a single instrument, such as secondary and backscattered electron imaging, electron backscatter diffraction, cathodoluminescence spectroscopy (CL) and energy dispersive x-ray spectroscopy (EDX) [4, 5]. A spatial resolution corresponding to the minimum diameter of the focused electron beam can, however, only be achieved for secondary electron imaging. The actual spatial resolution of analytical techniques such as x-ray and CL spectroscopy is governed by the interaction of the primary high-energy electrons with matter. Elastic and inelastic scattering of these electrons leads to a cascade of subsequent excitations in the material such as excited atomic shell electrons (resulting in characteristic x-ray radiation), plasmons, and hot electron-hole pairs (resulting in CL emission after thermalization) within a generation volume that strongly depends on the energy of the impinging primary electrons [2, 6].

In the 1970s and 1980s, several empirical expressions have been proposed to approximate the spatial distribution of electron beam-generated excitations [7–11]. Akamatsu *et al.* [12]

were the first to derive an analytical expression of the generation volume based on Monte Carlo (MC) simulations. Since the 1990s, when personal computers became wide spread, user friendly MC programs for the simulation of the generation volume have been developed, which are now widely used in the SEM community [13–17]. Invariably, the generation volume is assumed to be given by the total electron energy loss distribution, regardless of the electron energies actually involved in the detected radiation. However, whereas characteristic x-ray radiation (detected in EDX) is only excited by electrons with a kinetic energy on the order of 1 keV and higher [18], the radiative recombination of electron-hole pairs (detected in CL) only takes place between *thermalized* electron and hole populations. It is intuitively clear that the generation volume should be larger in the latter case. At sufficiently low energies (< 20 eV), the thermalization of electrons and holes with the lattice occurs predominantly via the electron-phonon, and particularly the Fröhlich interaction [19–21], which depends explicitly on temperature. MC programs such as CASINO [14–17], however, do not allow us to consider this carrier thermalization process since they ignore temperature-dependent phenomena altogether.

In the present work, we are interested in the generation volume relevant for CL spectroscopy, with the ultimate aim to reliably extract the carrier diffusion length in appropriately designed CL experiments. In the present article (the first of a series of three papers, hereafter referred to as CD1, CD2, and CD3), we first experimentally investigate the lateral extent of the CL generation volume in both GaN and GaAs. To this end, we use the CL emission from a single quantum well (QW) embedded in the GaN or GaAs matrix and clad by thin (Al,Ga)N or (Al,Ga)As barriers preventing carrier capture from the matrix by diffusion as originally proposed by Bonard *et al.* [22]. In other words, the QW emission is produced exclusively by direct carrier generation within

\* Present address: Istituto per la Microelettronica e Microsistemi, Consiglio Nazionale delle Ricerche, via del Fosso del Cavaliere 100, 00133 Roma, Italy

† [oliver.brandt@pdi-berlin.de](mailto:oliver.brandt@pdi-berlin.de)

the QW structure, while thermalized carriers in the GaN or GaAs matrix cannot contribute to it. These results will be used in two subsequent studies of the temperature-dependent carrier diffusion in GaN presented in the companion papers CD2 [23] and CD3 [24].

For the present paper, we record CL line scans intersecting the single QWs embedded in GaN or GaAs for various temperatures. The resulting CL intensity profiles are compared with MC simulations utilizing CASINO [16]. All experimental profiles turn out to be wider than the calculated ones, and their width increases further with decreasing temperature. Furthermore, the broadening at low temperatures becomes more pronounced for increasing acceleration voltages. The comparison of the results obtained on the two different materials helps to gain an understanding of the mechanisms giving rise to these effects. In particular, we attribute the broadening to the suppression of electron-phonon scattering processes with decreasing temperature, and its dependence on acceleration voltage to the slow-down of carrier cooling due to hot phonons. Finally, we present a phenomenological model reproducing the experimental profiles with a single free parameter that we employ to determine the diffusion length in the following papers CD2 [23] and CD3 [24].

## II. PRELIMINARY CONSIDERATIONS

The configuration of our CL experiment is displayed schematically in Fig. 1(a). The focused electron beam impinges onto the cross-section of the sample along the  $z$  direction. The beam and thus the carrier generation volume  $Q(x, y, z)$  (source) is scanned across the QW along the  $x$  axis normal to the well plane, with the center of the well being situated at  $x = 0$ . Since additional barriers of width  $b$  [cf. Fig. 1(b)] prevent a capture of thermalized diffusing carriers, only carriers excited within the barriers or directly within the QW with width  $2w$  can contribute to the detected CL signal of the QW.

According to the configuration of our experiment, we can consider the generation volume as a one-dimensional source after integrating over the  $y$  and  $z$  coordinates:

$$\bar{Q}(x) = \int_{-\infty}^{\infty} dy \int_0^{\infty} dz Q(x, y, z). \quad (1)$$

When this source is approaching the QW plane, the total flux of excited carriers captured by the well and thus the detected QW CL intensity  $\mathcal{F}(x)$  can be written as a convolution

$$\mathcal{F}(x) = \int_0^{\infty} \bar{Q}(x - x') F(x') dx', \quad (2)$$

with the function  $F(x')$  representing the fraction of carriers generated at  $x'$  and reaching the well.  $F(x')$  automatically

includes all carriers excited directly in the QW. For carriers excited within the barriers, we consider three different cases:

(i) Carriers generated in the barriers are localized and do not reach the well. In this case  $F(x') = F_0(x') = \delta(x')$  and the flux to the well is simply  $\mathcal{F}(x) = \mathcal{F}_0(x) = \bar{Q}(x)$ , where we have neglected the well width compared to the barrier width.

(ii) Carriers generated in the barriers can escape towards both the well and the matrix material. If the carrier diffusion length in the barrier is large compared to the barrier width, the fluxes to the well and to the matrix are weighted by the distance from the excitation position to the corresponding edges and can be written as:

$$F(x) = F_w(x) = \begin{cases} 1 - |x|/b, & |x| \leq b \\ 0, & |x| > b \end{cases}. \quad (3)$$

(iii) All carriers generated in the barriers are captured by the well and produce the maximum possible flux. Then, the flux to the well is written as:

$$F(x) = F_m(x) = \begin{cases} 1, & |x| \leq b \\ 0, & |x| > b \end{cases}. \quad (4)$$

We will first examine the influence of these different assumptions on the line profile for both GaN and GaAs. Let us assume that the initial distribution of carriers  $Q(x, y, z)$  generated by the electron beam is given by the energy loss distribution of the incident electrons. This loss distribution is calculated using CASINO [16], considering an  $\text{In}_{0.16}\text{Ga}_{0.84}\text{N}/\text{Al}_{0.11}\text{Ga}_{0.89}\text{N}$  and a  $\text{GaAs}/\text{Al}_{0.4}\text{Ga}_{0.6}\text{As}$  single QW with a width  $2w = 3$  and  $7$  nm, respectively, clad by barriers with a width  $b = 15$  nm. The acceleration voltage  $V$  of the electron beam and the beam diameter are set to  $5$  kV and  $5$  nm, respectively. Figures 2(a) and 2(b) show the simulated intensity profiles of the CL of the GaN- and GaAs-based QWs, respectively, considering the three different cases discussed above. The profiles resulting from the assumption in case (i) are clearly narrower than those obtained by considering the contribution of the barriers in cases (ii) and (iii). Evidently, the impact of carriers excited in the barriers and transferred to the well is significant, and must not be ignored. However, the profiles taking into account the contributions from the barriers according to cases (ii) or (iii) differ only marginally. In the following, we take case (iii) representing the maximum possible broadening of the energy loss profile simulated by CASINO.

## III. EXPERIMENT

For the experimental determination of the lateral extent of the CL generation volume, i. e., of  $\mathcal{F}(x)$  in GaN and GaAs, we synthesized single QW structures for both materials systems by molecular beam epitaxy. The former consists of a  $3$ -nm-thick  $\text{In}_{0.16}\text{Ga}_{0.84}\text{N}$  well clad by  $15$ -nm-thick

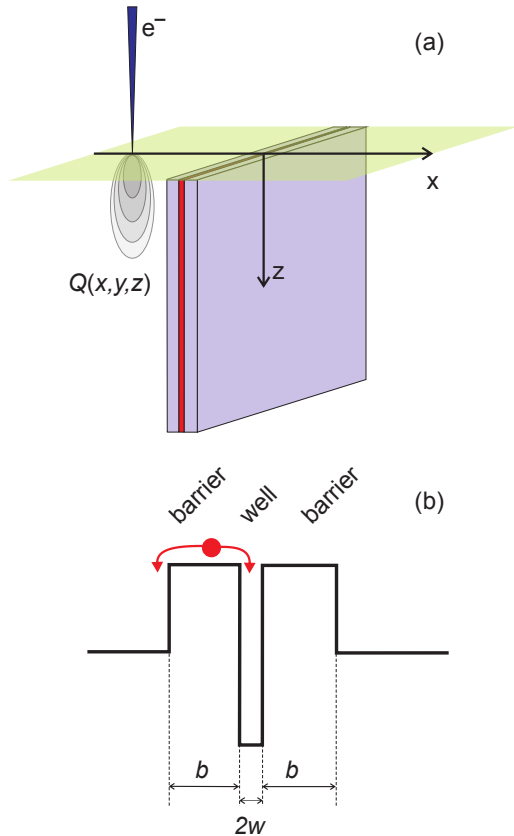


FIG. 1. (a) Configuration of the CL experiment with the electron beam scanning across the QW of width  $2w$  sandwiched between barriers of width  $b$ . (b) Sketch of the corresponding conduction band profile.

$\text{Al}_{0.11}\text{Ga}_{0.89}\text{N}$  barriers, embedded in a 1.3- $\mu\text{m}$ -thick GaN layer. This structure was synthesized on top of a GaN(0001) template prepared by metal-organic chemical vapor deposition on an  $\text{Al}_2\text{O}_3$ (0001) substrate. The latter structure contains a 7-nm-thick GaAs single QW clad by 15-nm-thick  $\text{Al}_{0.4}\text{Ga}_{0.6}\text{As}$  barriers within a 3- $\mu\text{m}$ -thick GaAs layer grown on a GaAs(001) substrate. In either case, we have chosen the structural and compositional parameters of the samples such as to inhibit thermionic injection and emission of carriers into and out of the QW, and to simultaneously ensure a sufficient spectral separation between the CL signals from the QW and the matrix.

The CL investigations were performed using a Gatan monoCL4 system and a He-cooling stage attached to a Zeiss Ultra55 SEM with a field emission gun. CL intensity profiles across the QW were obtained from CL photon counting maps of the cleaved edge of the two samples under investigation. Figures 3(a) and 3(b) show CL spectra of the GaN- and GaAs-related QWs, respectively, measured from a  $1\ \mu\text{m}^2$  region of the respective cross-section at low and elevated temperature. The spectral position of the (In,Ga)N/GaN QW CL band does not vary notably with varying temperature due to carrier localization effects. In order to cover the whole spectrum while acquiring photon counting maps of the QW

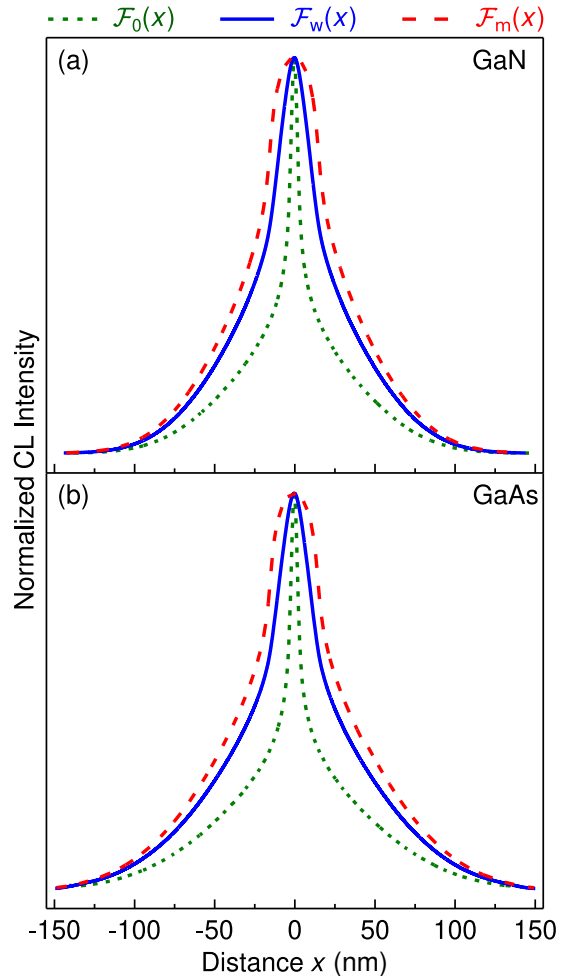


FIG. 2. Simulated CL profiles obtained from single QWs embedded in (a) GaN and (b) GaAs according to the experiment depicted in Fig. 1 and the three cases (i)–(iii) discussed in the text for  $V = 5\ \text{kV}$ . The center of the QW is situated at  $x = 0$ . The dotted lines show the profiles in case (i), which are given by the energy loss distribution of the incident electron beam  $\mathcal{F}_0(x) = \mathcal{Q}(x)$  calculated by CASINO [16] and integrated over the two coordinates  $y$  and  $z$  by Eq. (1). The solid lines depict the CL profile in case (ii) taking into account the diffusion of carriers generated within the barriers (barrier width  $b = 15\ \text{nm}$ ) towards the well and matrix material [ $\mathcal{F}_w(x)$ ]. For the dashed lines representing the profiles in case (iii), we assume that all carriers generated within the barriers are captured by the well [ $\mathcal{F}_m(x)$ ].

CL, the spectral window was set to 33 nm width as indicated in Fig. 3(a). The CL spectrum of the GaAs/(Al,Ga)As QW depicted in Fig. 3(b) shows a pronounced red-shift with increasing temperature and is superimposed by the emission spectrum of the GaAs matrix for  $T > 140\ \text{K}$ . For the acquisition of monochromatic CL maps of the GaAs/(Al,Ga)As QW, we used a spectral window of about 10 nm width as indicated in Fig. 3(b). We recorded CL profiles of the GaN- and GaAs-related QW for electron beam energies between 3 and 15 keV, with the beam current varying between 0.3 and 0.7 nA. The experiments were performed at sample tempera-

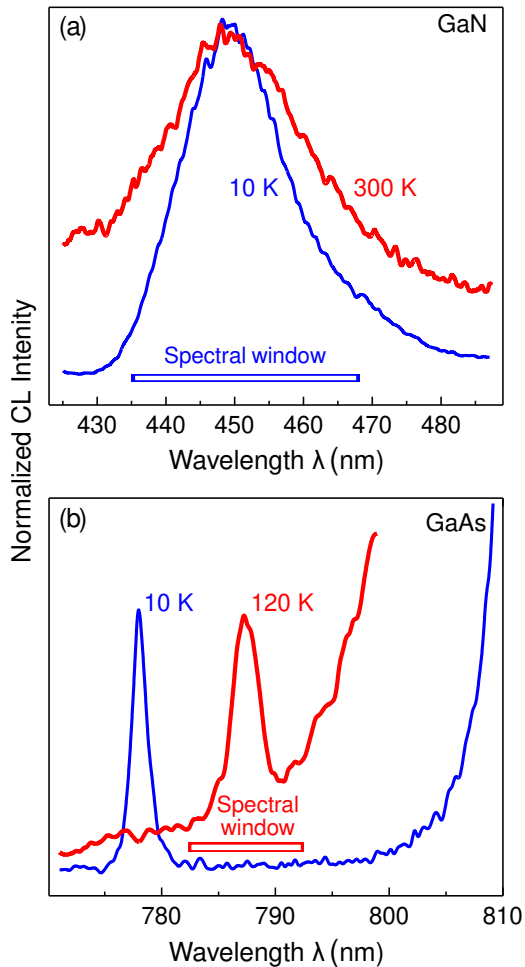


FIG. 3. CL spectra acquired at the cross-sections of single QWs embedded in (a) GaN and (b) GaAs for  $V = 5$  kV measured at low and elevated temperature. The spectral windows used for recording monochromatic CL photon counting maps such as depicted in Fig. 4(b) are indicated in the figure.

tures ranging from 10 to 300 K for the GaN- and 10 to 140 K for the GaAs-based QW.

#### IV. RESULTS AND DISCUSSION

##### A. Profiles of QW CL

Figures 4(a) and 4(b) display a secondary electron (SE) micrograph and a monochromatic CL photon counting map (central wavelength 450 nm), respectively, of the same cross-section region of the  $\text{In}_{0.16}\text{Ga}_{0.84}\text{N}/\text{Al}_{0.11}\text{Ga}_{0.89}\text{N}$  QW at 120 K and 5 kV. Due to the material contrast of the (Al,Ga)N barriers, the QW structure is clearly visible in the SE micrograph, where the high spatial resolution allows us to recognize even the 3-nm-thin QW in the center of the barrier-related dark stripe. The CL intensity map of Fig. 4(b) reflects the scattering of the incident electrons into the QW structure and is consequently much broader than the SE micrograph of

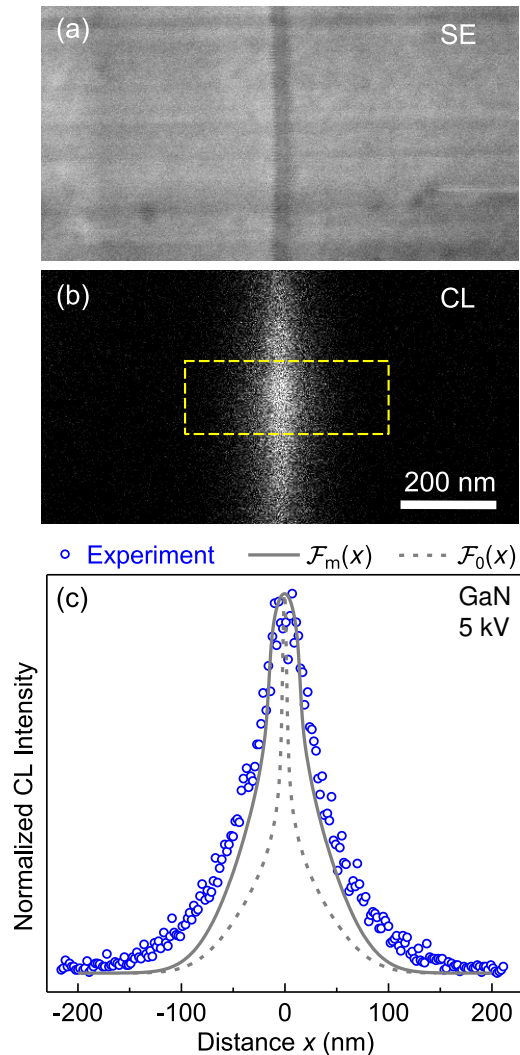


FIG. 4. (a) SE micrograph and (b) monochromatic CL photon counting map at  $\lambda = 450$  nm of the  $\text{In}_{0.16}\text{Ga}_{0.84}\text{N}/\text{Al}_{0.11}\text{Ga}_{0.89}\text{N}$  QW recorded at  $T = 120$  K and  $V = 5$  kV. In (b), the dashed rectangle indicates the window for the integration of the photon counts resulting in the experimental CL intensity profile. (c) Experimental CL intensity profile (symbols) extracted from the photon counting map in (b). The dashed and solid lines are the simulated profiles without  $[\mathcal{F}_0(x)]$  and with  $[\mathcal{F}_m(x)]$  taking into account carrier capture from the additional barriers, respectively.

the QW. CL intensity profiles are obtained by integrating the counts within a 130-nm-wide stripe-like window intersecting the QW as indicated in Fig. 4(b) by the dashed rectangle.

The symbols in Fig. 4(c) represent the experimental CL profile thus obtained. The dashed and solid lines of Fig. 4(c) are the simulated profiles based on CASINO without  $[\mathcal{F}_0(x)]$  and with  $[\mathcal{F}_m(x)]$  taking into account the profile broadening due to the presence of the barriers, respectively. This first example shows that even when accounting for the maximum broadening due to the barriers, the calculated profile is still slightly narrower than the experimental one.

Figures 5(a) and 5(b) depict CL intensity profiles of the



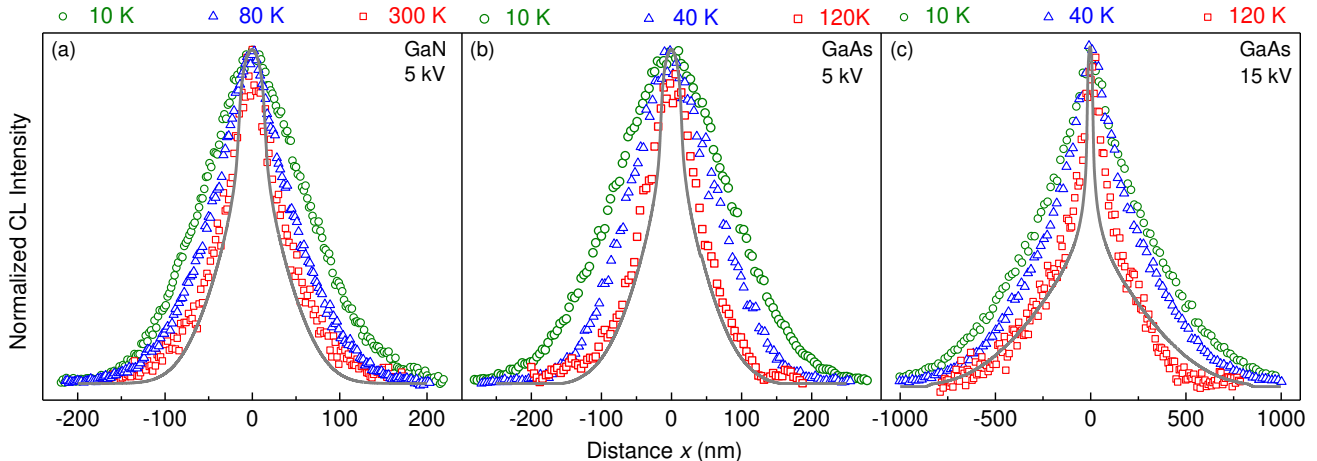


FIG. 5. Experimental CL profiles across the (a)  $\text{In}_{0.16}\text{Ga}_{0.84}\text{N}/\text{Al}_{0.11}\text{Ga}_{0.89}\text{N}$  QW at  $V = 5$  kV and (b)/(c)  $\text{GaAs}/\text{Al}_{0.4}\text{Ga}_{0.6}\text{As}$  QW at  $V = 5/15$  kV for different temperatures (symbols). The lines represent the simulated profiles  $\mathcal{F}_m(x)$  with the maximum width. Note the different  $x$  scale used in (c).

$\text{In}_{0.16}\text{Ga}_{0.84}\text{N}/\text{Al}_{0.11}\text{Ga}_{0.89}\text{N}$  and  $\text{GaAs}/\text{Al}_{0.4}\text{Ga}_{0.6}\text{As}$  QWs (symbols), respectively, recorded for different temperatures at  $V = 5$  kV. The solid lines are the simulated profiles with the maximum width [cf.  $\mathcal{F}_m(x)$  in Fig. 2]. For the highest temperatures (300 and 120 K for GaN and GaAs, respectively), these simulated profiles are only marginally narrower than the experimental ones. With decreasing temperatures, however, the measured CL profiles become progressively broader for both GaN and GaAs. The same effect is observed also at significantly higher acceleration voltages, as exemplified for the GaAs QW at  $V = 15$  kV in Fig. 5(c). While the relative change of the profile width is comparable to that observed for  $V = 5$  kV, the absolute one is larger.

The experimental data presented above demonstrate that the common perception of a temperature-independent generation volume in SEM, represented by the empirical energy loss distribution of the primary electrons as calculated, e. g., by CASINO, is incorrect as far as CL is concerned. Clearly, to account for our experimental findings, an additional temperature-dependent scattering mechanism has to be invoked that is not included in any of the presently available simulations of the generation volume in SEM. In the following, we will show that scattering of low-energy carriers by phonons is the most likely candidate for this mechanism.

### B. Electron-phonon scattering and CL profile width

In all applications of SEM, primary electrons are accelerated by voltages typically ranging from 1 to 30 kV. These primary electrons lose their energy once impinging onto the solid by a cascade of excitation processes, including high-energy events such as the excitation of core-level electrons, and low-energy events such as the excitation of plasmons that subsequently decay into hot electron-hole pairs, which in turn cool down by scattering with phonons. In MC programs such as CASINO, the spatial distribution of these

electron-hole pairs is represented by the total energy loss distribution of the impinging primary electrons calculated by empirical expressions [25], neglecting the energy relaxation and corresponding scattering events of the generated secondary carriers, and ignoring a potential dependence of these processes on temperature. This approximation is certainly justified for techniques for which low-energy electrons are irrelevant, such as for EDX. For CL, however, it has to be understood that efficient radiative recombination between electrons and holes only takes place when the respective carrier populations are close to thermalization with the lattice, i. e., when carriers have relaxed to their respective band edge in the vicinity of  $\mathbf{k} = 0$ . For energies below 20 eV, inelastic electron-electron scattering becomes rapidly inefficient with decreasing energy, and the energy loss rate of carriers is mainly determined by the Fröhlich interaction of electrons with longitudinal optical (LO) phonons [20]. For even lower energies, scattering with acoustic phonons contributes as well [26]. In any case, the cooling of hot carriers is accompanied by an expansion of their spatial distribution, which can be understood as a (super)-diffusive process [27, 28], but has to be distinguished from the normal diffusion of carriers in thermal equilibrium with the lattice. As a consequence of the inherent temperature dependence of electron-phonon scattering, we expect that the generation volume relevant for CL depends on temperature as well.

To see if this temperature dependence is qualitatively consistent with the effect observed experimentally, i. e., a widening of the profiles with decreasing temperature, we perform simple Monte Carlo simulations as described in detail in Appendix A. Note that these simulations are too crude to allow a quantitative comparison of the simulated and experimental profiles, because we neglect, for example, the band structure and phonon dispersion of the semiconductor [26], and the Coulomb interaction between electrons and holes that becomes important at lower energies [29]. We start with electrons with a spatial distribution as provided by CASINO

for  $V = 5$  kV, and a Gaussian energy distribution centered at half of the band gap energy of GaN. We next allow these electrons to cool down via the Fröhlich interaction for lattice temperatures of 30 and 300 K and an effective phonon energy [26] of 30 meV. The resulting one-dimensional distributions are displayed as dashed and solid lines in Fig. 6, respectively. The dotted curve represents the corresponding lateral distribution of the energy loss of the primary electrons  $\mathcal{F}_0(x)$  as calculated by CASINO. Evidently, our simple simulations qualitatively reproduce the main features observed experimentally: the cooling of hot carriers leads to a broadening of the energy loss profile, which is more pronounced at lower temperature. The simulations show that the reason underlying this effect is the increasing mean free length of carriers with decreasing temperature, which is determined almost exclusively by the lower probability of LO phonon emission.

Instead of attempting to predict the temperature-dependent CL generation volume theoretically, which would be a challenging task in itself, we will simply extract its one-dimensional lateral component from our experimental data. In fact, the measured intensity profiles displayed in Fig. 5 contain the information about the temperature dependence of the CL generation volume. Understanding the broadening due to carrier thermalization as an independent and statistical process, we can phenomenologically describe the resulting profile as a convolution of  $\mathcal{F}(x)$  and a Gaussian distribution  $\mathcal{G}(x)$  with the standard deviation  $\sigma$ . Then, the flux of the carriers to the well can be written analogously to Eq. (2),

$$\tilde{\mathcal{F}}(x) = \int_0^{\infty} \tilde{Q}(x-x')\tilde{F}(x')dx', \quad (5)$$

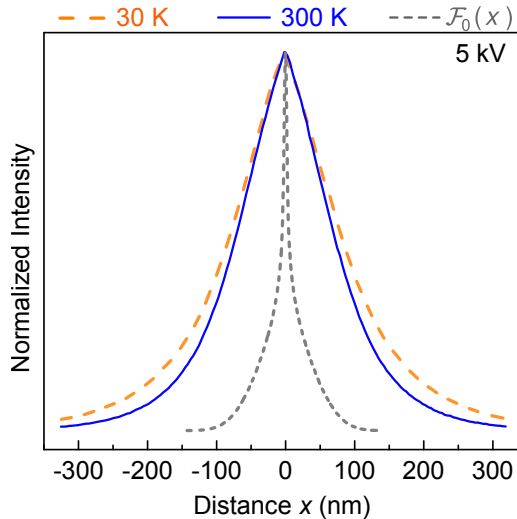


FIG. 6. Simulated lateral distributions of carriers after excitation of GaN at 5 kV and subsequent cooling at 30 (dashed line) and 300 K (solid line) explicitly taking into account the Fröhlich interaction as the sole inelastic scattering mechanism. The dotted curve depicts the initial lateral distribution of the energy loss  $\mathcal{F}_0(x)$  calculated by CASINO.

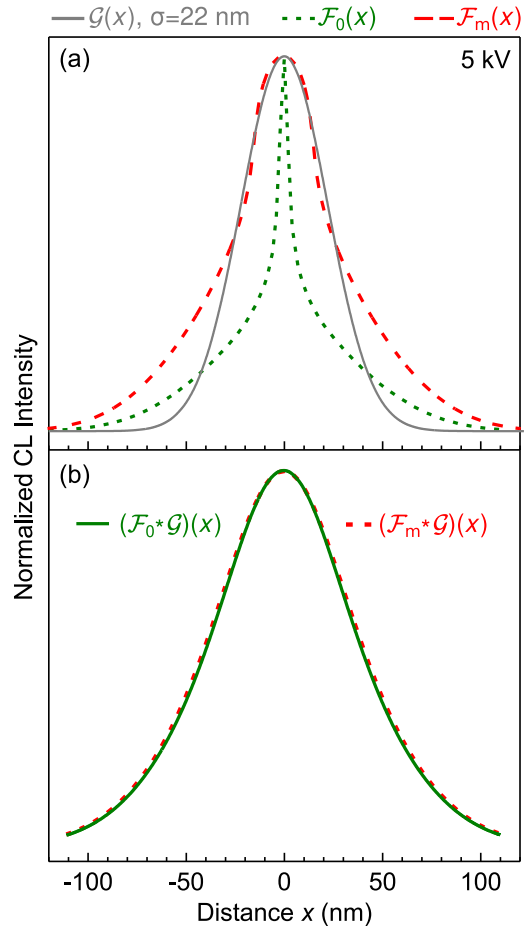


FIG. 7. (a) Intensity profiles given by the bare source  $\mathcal{F}_0(x)$  (dotted line) and by  $\mathcal{F}_m(x)$  taking into account the maximum broadening effect from the barriers (dashed line) for GaN and  $V = 5$  kV. The solid line depicts a Gaussian  $\mathcal{G}(x)$  of width  $\sigma = 22$  nm. (b) Convolution of  $\mathcal{F}_0(x)$  and  $\mathcal{F}_m(x)$  with  $\mathcal{G}(x)$  resulting in the solid and dashed line, respectively.

where the functions  $\tilde{F}(x')$  are obtained by a convolution of any of the three functions  $F(x')$  in Eq. (2) with a Gaussian. The respective convolution integrals are shown to be given in terms of the error function in Appendix B.

To illustrate this approach, we compare a simulation based on the source  $\mathcal{F}_0(x)$  with the corresponding one in which the maximum impact of barriers is taken into account via the distribution  $\mathcal{F}_m(x)$ . Figure 7(a) shows these distributions together with a Gaussian distribution  $\mathcal{G}(x)$  with  $\sigma = 22$  nm that we show below to be suitable for describing the room-temperature CL profile of the GaN-based QW [cf. Fig. 8(a)]. Figure 7(b) displays the results of the convolution of these distributions with the Gaussian after normalization. Surprisingly, the shape of these convolutions is almost identical, and is unaffected by the presence of the barriers. Hence, we can extract the actual lateral carrier distribution by fitting experimental CL intensity profiles by a convolution of the energy loss distribution  $\mathcal{F}_0(x)$  as obtained from CASINO and a Gaussian, with  $\sigma$  being the sole fit parameter. In this

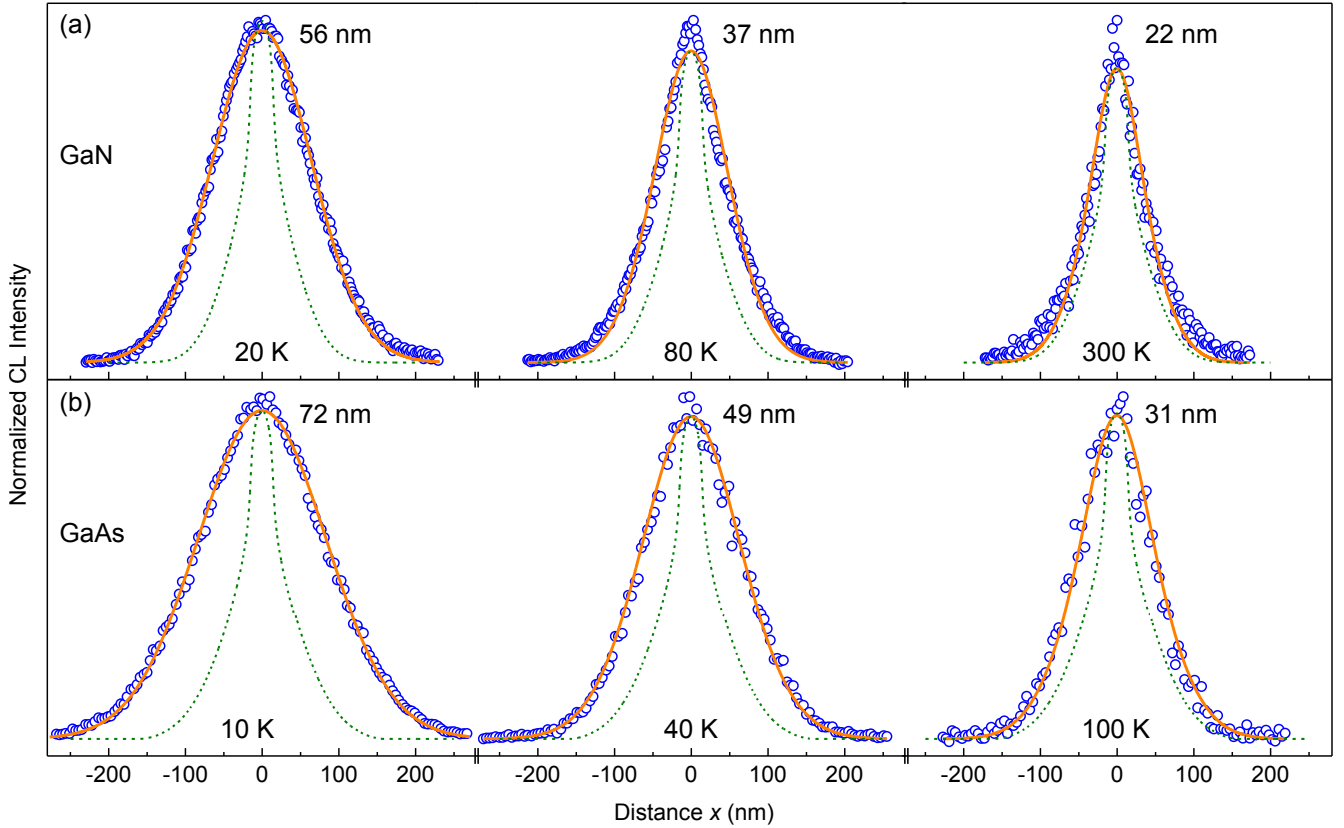


FIG. 8. Experimental CL profiles (symbols) across the (a)  $\text{In}_{0.16}\text{Ga}_{0.84}\text{N}/\text{Al}_{0.11}\text{Ga}_{0.89}\text{N}$  QW and (b)  $\text{GaAs}/\text{Al}_{0.4}\text{Ga}_{0.6}\text{As}$  QW acquired at  $V = 5$  kV and different temperatures as indicated in the figure. The solid lines are fits to the data implemented by a convolution of the source  $\mathcal{F}_0(x)$  with a Gaussian distribution  $\mathcal{G}(x)$  of width  $\sigma$  as indicated in the panels. The dotted curves represent  $\mathcal{F}_m(x)$  with the maximum source broadening.

way, it is straightforward to gather comprehensive information on the temperature- and voltage-dependent broadening of the source, and thus to establish an understanding of the mechanisms governing this broadening.

### C. Temperature and voltage dependence of the CL profile width

Figures 8(a) and 8(b) display experimental CL intensity profiles recorded at three different temperatures for both the GaN- and GaAs-based QWs, respectively. For both materials systems, the temperature-independent source  $\mathcal{F}_m(x)$  severely underestimates the lateral extent of the CL generation volume even at the highest temperature and deviates increasingly from the measured extent of the CL generation volume with decreasing temperature. The convolution of  $\mathcal{F}_0(x)$  with a Gaussian of width  $\sigma(T)$  as proposed above as a phenomenological means to describe the profiles yields indeed satisfactory fits for all temperatures and for both materials systems.

Figure 9 summarizes the results of the fits performed in this way for the GaN- and GaAs-based QWs between 10 and 300 K and an acceleration voltage of 5 kV. As discussed in

detail above, the values of  $\sigma$  represent the broadening of the source due to the cooling of hot carriers, and the temperature dependence of this broadening is primarily related to the decreasing LO phonon emission rate with decreasing temperature. For the beam energy of 5 kV chosen for these experiments, the absolute values of  $\sigma$  for the two samples are almost equal between 40 and 140 K, and becomes only slightly larger at lower temperatures for the QW embedded in GaAs. Overall, there seems to be no significant difference for the temperature-dependent broadening in the GaN- and GaAs-based QWs.

However, this impression changes when examining profiles acquired at different acceleration voltages. Figures 10(a) and 10(b) show  $\sigma(T)$  for the QWs embedded in GaAs and GaN, respectively, resulting from CL intensity profiles recorded with acceleration voltages between 3 and 15 kV. These plots demonstrate that the temperature dependencies of  $\sigma$  for the GaAs- and GaN-based QWs are in fact quite different. In particular, three characteristic differences are noted: (i) At elevated temperature,  $\sigma$  is essentially constant and amounts to about 30 nm for the GaAs-based and 20 nm for the GaN-based QW. (ii) At a characteristic temperature  $T_C$ ,  $\sigma$  starts to increase with decreasing temperature.  $T_C$  corresponds to about 80 K for the GaAs-based and 150 K for

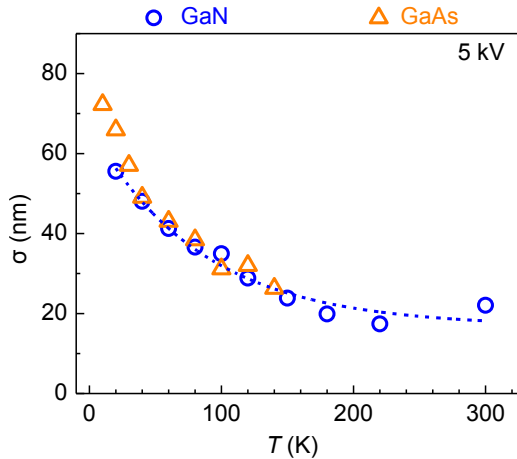


FIG. 9. Standard deviation  $\sigma$  of the Gaussian distribution  $\mathcal{G}(x)$  obtained by fits of experimental CL profiles as shown exemplarily in Fig. 8(a) and 8(b) as a function of  $T$  for the single QWs embedded in GaN (circles) and GaAs (triangles). The dotted line is a guide to the eye.

the GaN-based QW independent of acceleration voltage. (iii) For  $T < T_C$ ,  $\sigma$  increases stronger with acceleration voltage for the GaN-based as compared to the GaAs-based QW. The inset in (b) reveals that  $\sigma$  increases almost linearly with  $V$  for the GaN-based QW at 10 K.

At the first glance, the strong dependence of the temperature-dependent broadening of the profiles on the acceleration voltage or beam energy is puzzling, since the cooling of hot secondary electrons and holes by LO phonon emission is not expected to retain a memory of the energy of the primary electrons. However, even for a constant beam current, higher beam energies are inevitably accompanied by a higher density of secondary electrons and holes, and the cooling of hot carriers, or more precisely their energy loss rate, is known to depend on their density. In fact, experiments utilizing both continuous wave and pulsed laser excitation of semiconductors have shown that the energy loss rate of hot carriers decreases roughly linearly with increasing photogenerated carrier density [30–34]. For GaAs, for example, the energy loss rate is reduced by one (two) orders of magnitude for a carrier density of  $10^{17}$  ( $10^{18}$ )  $\text{cm}^{-3}$ . This effect is caused by hot carriers cooling down via the emission of LO phonons, thus creating a nonequilibrium population of hot LO phonons [31, 35, 36] that in turn heats the carrier distribution by strongly increasing the probability of LO phonon absorption. As a consequence, carrier cooling slows down, causing a further quasi-diffusive broadening of the initial secondary carrier distribution.

In the present experiments, four factors influence the cathodogenerated carrier density: (i) the beam energy, with which the carrier density increases roughly linearly, and which was here varied by a factor of 5, (ii) the beam current, which usually increases sublinearly with the beam energy, and was here varied by a factor of 2 between 3 and 15 kV, (iii) the carrier lifetime, which depends strongly on temper-

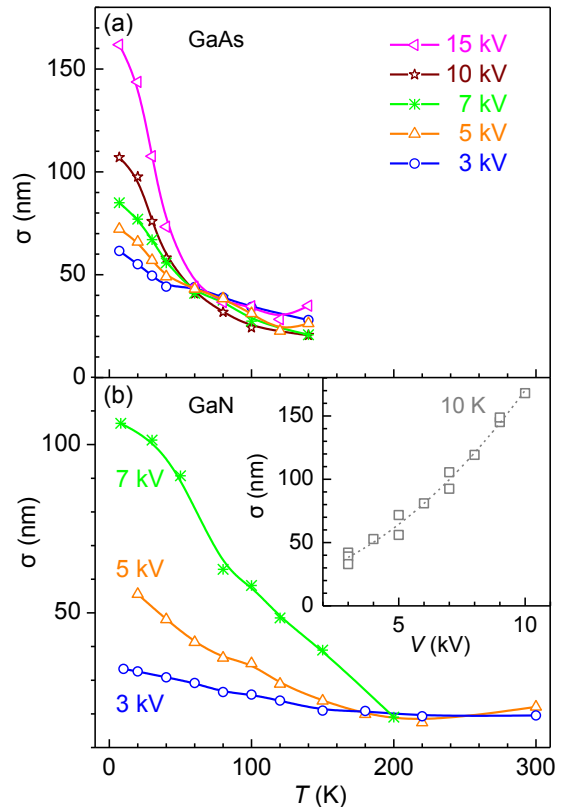


FIG. 10. Standard deviation  $\sigma$  of the Gaussian distribution  $\mathcal{G}(x)$  obtained by fits of experimental CL profiles as a function of  $T$  for various acceleration voltages of the primary electrons (a) for the GaAs- and (b) the GaN-based QW. The lines serve as guide to the eye. The inset in (b) shows the dependence of  $\sigma$  on acceleration voltage for the GaN-based QW at 10 K.

ature, but also on carrier density, and which we measured to increase by a factor of 5 for the GaN matrix between 300 and 10 K, and (iv) the contribution of surface recombination, which is reduced with an increasing depth of excitation for larger beam energies. Taking all of these factors into account, the carrier density in our experiments is expected to increase by roughly two orders of magnitude between measurements taken at 300 K and 3 kV compared to 10 K and 15 kV. In terms of absolute numbers, we estimate that the minimum and maximum cathodogenerated carrier density is on the order of  $10^{17}$  and  $10^{19}$   $\text{cm}^{-3}$ , respectively.

Finally, the characteristic differences in  $\sigma(T)$  of GaAs and GaN listed above can be understood in terms of the different LO phonon energy (36 and 92 meV, respectively) and effective strength of the electron-LO phonon coupling  $\alpha$  (0.068 [37] and 0.44 [38], respectively) in these two materials. The former is likely to be responsible for the difference in the onset of the broadening at lower temperatures, while the latter determines the dependence of the broadening on carrier density. In fact, the reduction of the energy loss rate by hot phonons depends on the Fröhlich coupling constant: the stronger the coupling, the slower is the cooling. This relation has been demonstrated in a comparative study of the cooling



of hot carriers in CdSe and GaAs, where the energy loss rate in CdSe was found to be reduced by hot phonon effects ten times more than in GaAs due to the stronger electron-LO phonon coupling in this more ionic II-VI semiconductor ( $\alpha \approx 0.2$  for CdSe) [39].

## V. SUMMARY AND CONCLUSIONS

Our study has shown that the paradigm of a temperature-independent generation volume applicable to all SEM-based techniques needs to be revised. While Monte Carlo simulations based on empirical energy loss expressions such as that implemented in CASINO describe the generation volume relevant for EDX very well, this generation volume is not the one relevant for CL. In fact, we have shown that the latter depends strongly on temperature, with a broadening that increases with decreasing temperature. This effect is understood when considering that radiative recombination of charge carriers in semiconductors takes place between thermalized electron-hole populations in the vicinity of  $\mathbf{k} = 0$ . The mean free path of carriers relaxing to their respective band edges is controlled by carrier-phonon scattering, and thus increases with decreasing temperature. In addition, we have found this phenomenon to be more pronounced for higher beam energies, which we attribute to a marked slow-down of carrier relaxation due to the non-equilibrium phonon population (hot phonons) building up with increasing carrier density.

In view of the considerable complexity of the energy relaxation of hot carriers in semiconductors, we have not attempted to develop a unified framework embracing the initial high-energy loss processes and the subsequent thermalization and cooling of hot carriers, but have opted for a phenomenological approach capable of approximating the temperature- and voltage-dependent lateral generation profiles reasonably well. We have shown that this goal can be achieved by convoluting the energy loss profile computed by CASINO with a Gaussian of variable standard deviation. We will use this methodology in the companion papers CD2 and CD3 for a reliable experimental determination of the temperature-dependent diffusivity in GaN.

## ACKNOWLEDGMENTS

The authors are indebted to Achim Trampert for a critical reading of the manuscript. U.J. thanks Holger T. Grahn for his continuous encouragement and support. K. K. S. and A. E. K. acknowledge the support of the Russian Science Foundation under grant N 19-11-00019.

### Appendix A: Carrier cooling via LO phonon scattering

We assume the energy loss distribution as computed by CASINO to represent the initial spatial distribution of electrons (or holes). For constructing a situation in which all

secondary excitations have energies below the impact ionization threshold, so that a generation of further electron-hole pairs cannot occur, we assume their energy distribution to be given by  $\exp[-(E - E_0)^2 / \Delta E^2]$  with the electron energy  $E$ ,  $E_0 = 1.75$  eV, and  $\Delta E = 1$  eV. To participate in radiative recombination with likewise thermalized holes, these electrons have to relax to the bottom of the conduction band. For simplicity, we ignore that the thermalization takes place in a semiconductor with a complex band structure and phonon dispersion, and assume instead that momentum conservation is automatically fulfilled, and that thermalization occurs by the interaction of electrons having a constant mass  $m^* = m_0$  equal to that of free electrons with phonons of an (effective) [26] energy of 30 meV. To follow the evolution of the energy and the position of each electron during its energy relaxation process, we perform Monte Carlo calculations in the spirit of those described in Refs. [19–21].

The mean free path of the electron between electron-phonon collisions is  $\lambda = v/(W^+ + W^-)$  with the electron velocity  $v = (2E/m_0)^{1/2}$ , and the rates for phonon absorption and emission

$$W^- = \frac{n_{ph}}{a_{BK}} \frac{E_{ph}}{\sqrt{2Em^*}} \ln \left( \frac{[1 + E_{ph}/E]^{1/2} + 1}{[1 + E_{ph}/E]^{1/2} - 1} \right), \quad (A1)$$

and

$$W^+ = \frac{n_{ph} + 1}{a_{BK}} \frac{E_{ph}}{\sqrt{2Em^*}} \ln \left( \frac{1 + [1 - E_{ph}/E]^{1/2}}{1 - [1 - E_{ph}/E]^{1/2}} \right), \quad (A2)$$

respectively. Here,  $E_{ph} = 0.03$  eV is the effective phonon energy,  $a_B$  is the Bohr radius,  $n_{ph} = \left( e^{E_{ph}/k_B T} - 1 \right)^{-1}$  is the equilibrium phonon occupation number, and  $\kappa = (1/\epsilon_\infty - 1/\epsilon_s)^{-1} = 11.8$  with the high frequency and the static relative permittivities  $\epsilon_\infty$  and  $\epsilon_s$ , respectively.

Finally, the angular distribution of electrons scattered by phonons is given by the probability of scattering between  $\theta$  and  $\theta + d\theta$  proportional to

$$\frac{\sqrt{E'} \sin \theta d\theta}{E + E' - 2\sqrt{EE'} \cos \theta}, \quad (A3)$$

where  $E$  and  $E'$  are the electron energies before and after the scattering event.

### Appendix B: Model description of the lateral carrier distribution

Since a comprehensive description of the distribution of thermalized carriers produced by the electron beam is a highly complex problem, we model the source of carriers by assuming a Gaussian broadening of the energy loss dis-

tribution  $Q(x, y, z)$  (that is calculated by CASINO), so that

$$\begin{aligned} \tilde{Q}(x, y, z) = & \iint_{-\infty}^{\infty} dx' dy' Q(x', y', z) \\ & \times \exp \left[ -\frac{(x-x')^2 + (y-y')^2}{2\sigma^2} \right]. \end{aligned} \quad (\text{B1})$$

In this model, we include convolutions over  $x$  and  $y$  but not over  $z$ , since the energy loss distribution  $Q(x, y, z)$  is much broader in depth  $z$  as compared with its width in the lateral directions  $x, y$  and the actual standard deviation  $\sigma$  required to match the experiment.

Our aim is to determine the total flux of the carriers  $\tilde{F}(x)$  to the quantum well as a function of the current position  $x$  of the electron beam that scans along the surface. This flux is a result of the generation of carriers both directly in the well and in the barriers produced by a source  $\tilde{Q}(x - x', y, z)$ , where  $x - x'$  are positions of the points in the source with respect to its center along the scan direction. As we have already discussed above, the  $y$ - and  $z$ -positions of the excitation points are not essential when calculating the total flux. We can consider a one-dimensional diffusion problem

with the source

$$\tilde{Q}(x - x') = \int_{-\infty}^{\infty} dy \int_0^{\infty} dz \tilde{Q}(x - x', y, z) \quad (\text{B2})$$

and, collecting contributions from the carriers excited at all positions  $x'$ , represent the total flux as a convolution

$$\tilde{F}(x) = \int_{-\infty}^{\infty} dx' \tilde{Q}(x - x') F(x'). \quad (\text{B3})$$

The function  $F(x')$  is either equal to  $F_w(x')$  [Eqs. (3)] or  $F_m(x')$  [Eqs. (4)]. Using equations (B1), (B2), and (B3) and changing the sequence of integrations, we can write the total flux as a convolution

$$\tilde{F}(x) = \int_{-\infty}^{\infty} dx' \tilde{Q}(x - x') \tilde{F}(x') \quad (\text{B4})$$

with

$$\tilde{F}(x) = \int_{-\infty}^{\infty} dx' F(x') \exp \left[ -\frac{(x-x')^2}{2\sigma^2} \right]. \quad (\text{B5})$$

The integrals with the functions  $F(x)$  given by Eqs. (3) and (4) can be calculated analytically. For  $F(x') = F_w(x')$ , we get from Eq. (3)

$$\begin{aligned} \tilde{F}_w(x) = & \frac{\sigma}{2b} \left\{ \sqrt{2\pi} \left[ (b-x) \operatorname{erf} \left( \frac{b-x}{\sqrt{2}\sigma} \right) - 2x \operatorname{erf} \left( \frac{x}{\sqrt{2}\sigma} \right) + (b+x) \operatorname{erf} \left( \frac{b+x}{\sqrt{2}\sigma} \right) \right] \right. \\ & \left. + 2\sigma \left[ \exp \left( -\frac{(b-x)^2}{2\sigma^2} \right) - 2 \exp \left( -\frac{x^2}{2\sigma^2} \right) + \exp \left( -\frac{(b+x)^2}{2\sigma^2} \right) \right] \right\}, \end{aligned} \quad (\text{B6})$$

where  $\operatorname{erf}(x)$  is the error function.

For  $F(x') = F_m(x')$ , we obtain from Eq. (4)

$$\tilde{F}_m(x) = \sigma \sqrt{\frac{\pi}{2}} \left[ \operatorname{erf} \left( \frac{b-x}{\sqrt{2}\sigma} \right) + \operatorname{erf} \left( \frac{b+x}{\sqrt{2}\sigma} \right) \right]. \quad (\text{B7})$$

- 
- [1] L. Reimer, *Scanning Electron Microscopy*, edited by P. W. Hawkes and H. K. V. Lotsch, Springer Series in Optical Sciences, Vol. 45 (Springer-Verlag, Berlin Heidelberg, 1998).  
 [2] J. I. Goldstein, D. E. Newbury, J. R. Michael, N. W. Ritchie, J. H. J. Scott, and D. C. Joy, *Scanning Electron Microscopy and X-Ray Microanalysis* (Springer Science + Business Media,

- New York, 2003).  
 [3] W. Zhou and Z. L. Wang, *Scanning Microscopy for Nanotechnology: Techniques and Applications* (Springer, New York, 2007).  
 [4] T. Coenen and N. M. Haegel, Cathodoluminescence for the 21st century: Learning more from light, *Appl. Phys. Lett.* **4**,

- 031103 (2017).
- [5] W.-H. Lin, U. Jahn, H. Küpers, E. Luna, R. B. Lewis, L. Geelhaar, and O. Brandt, Efficient methodology to correlate structural with optical properties of GaAs nanowires based on scanning electron microscopy, *Nanotechnology* **28**, 415703 (2017).
- [6] P. R. Edwards and R. W. Martin, Cathodoluminescence nanocharacterization of semiconductors, *Semicond. Sci. Technol.* **26**, 064005 (2011).
- [7] T. E. Everhart and P. H. Hoff, Determination of kilovolt electron energy dissipation vs penetration distance in solid materials, *J. Appl. Phys.* **42**, 5837 (1971).
- [8] H.-J. Fitting, H. Glaefcke, and W. Wild, Electron penetration and energy transfer in solid targets, *Phys. Status Solidi B* **43**, 185 (1977).
- [9] C. Donolato, An analytical model of SEM and STEM charge collection images of dislocations in thin semiconductor layers: I. Minority carrier generation, diffusion, and collection, *Phys. Status Solidi A* **65**, 649 (1981).
- [10] G. Oelgart and U. Werner, Kilovolt electron energy loss distribution in GaAsP, *Phys. Status Solidi A* **85**, 205 (1984).
- [11] U. Werner, F. Koch, and G. Oelgart, Kilovolt electron energy loss distribution in Si, *J. Phys. Appl. Phys.* **21**, 116 (1988).
- [12] B. Akamatsu, P. Henoc, and R. B. Martins, Caractérisation des dispositifs opto-électroniques par microscopie à balayage, *J. Microsc. Spectrosc. Electron.* **14**, 12a (1989).
- [13] D. B. Holt and E. Napchan, Quantitation of SEM EBIC and CL signals using Monte Carlo electron-trajectory simulations, *Scanning* **16**, 78 (1994).
- [14] P. Hovington, D. Drouin, and R. Gauvin, CASINO: A new Monte Carlo code in C language for electron beam interaction—Part I: Description of the program, *Scanning* **19**, 1 (1997).
- [15] D. Drouin, P. Hovington, and R. Gauvin, CASINO: A new Monte Carlo code in C language for electron beam interactions—Part II: Tabulated values of the Mott cross section, *Scanning* **19**, 20 (1997).
- [16] D. Drouin, A. R. Couture, D. Joly, X. Tastet, V. Aimez, and R. Gauvin, CASINO V2.42—A fast and easy-to-use modeling tool for scanning electron microscopy and microanalysis users, *Scanning* **29**, 92 (2007).
- [17] H. Demers, N. Poirier-Demers, A. R. Couture, D. Joly, M. Guilmain, N. de Jonge, and D. Drouin, Three-dimensional electron microscopy simulation with the CASINO Monte Carlo software, *Scanning* **33**, 135 (2011).
- [18] E. D. Boyes, On low voltage scanning electron microscopy and chemical microanalysis, *Microsc. Microanal.* **6**, 307 (2000).
- [19] J. Llacer and E. L. Garwin, Electron-Phonon interaction in alkali halides. I. The transport of secondary electrons with energies between 0.25 and 7.5 eV, *J. Appl. Phys.* **40**, 2766 (1969).
- [20] M. Dapor, Monte Carlo simulation of secondary electron emission from dielectric targets, *J. Phys. Conf. Ser.* **402**, 012003 (2012).
- [21] M. Dapor, *Transport of Energetic Electrons in Solids*, 2nd ed., Springer Tracts in Modern Physics, Vol. 999 (Springer International Publishing, Cham, 2017).
- [22] J.-M. Bonard, J.-D. Ganière, B. Akamatsu, D. Araújo, and F.-K. Reinhart, Cathodoluminescence study of the spatial distribution of electron-hole pairs generated by an electron beam in  $\text{Al}_{0.4}\text{Ga}_{0.6}\text{As}$ , *J. Appl. Phys.* **79**, 8693 (1996).
- [23] O. Brandt, V. M. Kaganer, J. Lähnemann, T. Flissikowski, C. Pfüller, K. K. Sabelfeld, A. Kireeva, C. Chèze, R. Calarco, H. T. Grahn, and U. Jahn, Carrier diffusion in GaN—a cathodoluminescence study. II: Ambipolar vs. exciton diffusion, unpublished (2020).
- [24] J. Lähnemann, V. M. Kaganer, K. K. Sabelfeld, A. Kireeva, U. Jahn, C. Chèze, R. Calarco, O. Brandt, R. Calarco, H. T. Grahn, and U. Jahn, Carrier diffusion in GaN—a cathodoluminescence study. III: Nature of nonradiative recombination at threading dislocations, unpublished (2020).
- [25] D. C. Joy and S. Luo, An empirical stopping power relationship for low-energy electrons, *Scanning* **11**, 176 (1989).
- [26] V. P. Zhukov, V. G. Tyuterev, E. V. Chulkov, and P. M. Echenique, Electron-phonon relaxation and excited electron distribution in gallium nitride, *J. Appl. Phys.* **120**, 085708 (2016).
- [27] M. Kozák, F. Trojánek, and P. Malý, Hot-carrier transport in diamond controlled by femtosecond laser pulses, *New J. Phys.* **17**, 053027 (2015).
- [28] E. Najafi, V. Ivanov, A. Zewail, and M. Bernardi, Superdiffusion of excited carriers in semiconductors, *Nat. Commun.* **8**, 1 (2017).
- [29] P. E. Selbmann, M. Gulia, F. Rossi, E. Molinari, and P. Lugli, Coupled free-carrier and exciton relaxation in optically excited semiconductors, *Phys. Rev. B* **54**, 4660 (1996).
- [30] R. F. Leheny, J. Shah, R. L. Fork, C. V. Shank, and A. Migus, Dynamics of hot carrier cooling in photo-excited GaAs, *Solid State Commun.* **31**, 809 (1979).
- [31] P. Lugli, C. Jacoboni, L. Reggiani, and P. Kocevar, Monte Carlo algorithm for hot phonons in polar semiconductors, *Appl. Phys. Lett.* **50**, 1251 (1987).
- [32] H. Lobentanzer, H.-J. Pollard, W. W. Rühle, W. Stolz, and K. Ploog, Cooling of an electron-hole plasma in a  $\text{Ga}_{0.47}\text{In}_{0.53}\text{As}$  multiple-quantum-well structure, *Phys. Rev. B* **36**, 1136 (1987).
- [33] K. Leo, W. W. Rühle, and K. Ploog, Hot-carrier energy-loss rates in  $\text{GaAs}/\text{Al}_x\text{Ga}_{1-x}\text{As}$  quantum wells, *Phys. Rev. B* **38**, 1947 (1988).
- [34] M. C. Marchetti and W. Pötz, Relaxation of photoexcited electron-hole plasma in quantum wells, *Phys. Rev. B* **40**, 12391 (1989).
- [35] J. Shah, R. C. C. Leite, and J. F. Scott, Photoexcited hot LO phonons in GaAs, *Solid State Commun.* **8**, 1089 (1970).
- [36] J. Shah, Hot carriers in quasi-2-D polar semiconductors, *IEEE J. Quantum Electron.* **22**, 1728 (1986).
- [37] K. J. Nash, M. S. Skolnick, and S. J. Bass, Electron-phonon interactions in indium gallium arsenide, *Semicond. Sci. Technol.* **2**, 329 (1987).
- [38] A. S. Barker and M. Ilegems, Infrared lattice vibrations and free-electron dispersion in GaN, *Phys. Rev. B* **7**, 743 (1973).
- [39] S. S. Prabhu, A. S. Vengurlekar, S. K. Roy, and J. Shah, Nonequilibrium dynamics of hot carriers and hot phonons in CdSe and GaAs, *Phys. Rev. B* **51**, 14233 (1995).